

Imaginary-Temperature Zeros for Quantum Phase Transitions

Jinghu Liu¹, Shuai Yin^{2,*} and Li Chen^{1†}

¹*Institute of Theoretical Physics, State Key Laboratory of Quantum Optics and Quantum Optics Devices, Shanxi University, Taiyuan 030006, China*

²*School of Physics, Sun Yat-Sen University, Guangzhou 510275, China*

While the zeros of complex partition functions, such as Lee-Yang zeros and Fisher zeros, have been instrumental in characterizing temperature-driven phase transitions, the extension of this concept to zero temperature remains an open and active topic. In this paper, we introduce the concept of *Imaginary-Temperature Zeros* (ITZs) by calculating the zeros of the *imaginary-temperature partition function*. We delve into the properties of ITZs for the transverse-field Ising chain, and find that the ITZs are distributed in sectorial structures, accompanied by universal singular behaviors for such quantities as the edge density of ITZs and the magnetization. These singularities remarkably differ from those in the Lee-Yang theory, and are demonstrated to be intimately related to quantum criticality and the Ising critical exponents. We further illuminate the correspondence between ITZs and the zeros of the spectrum form factor, which offers a practical way for detecting ITZs and zero-temperature phase transitions through quantum dynamics.

Introduction. The importance of complex quantities cannot be overstated in physics. In quantum mechanics, for instance, complex numbers are essential for capturing the physical reality of nature. Besides, complex quantities also play radical roles in statistical physics. By extending the symmetry-breaking field h to the complex domain, Lee and Yang found that the zeros of the complex-valued partition function of the classical Ising model [1, 2], known as Lee-Yang zeros, reside in a unit circle of $x = e^{\beta h}$, where β is the inverse temperature. In the thermodynamic limit, Lee-Yang zeros approach the real axis, serving as an unambiguous sign of thermal phase transitions. Hence, Lee-Yang theory established the mechanism for signifying phase transitions from the fundamental ensemble theory of statistical mechanics. Later on Fisher extended this concept by considering the zeros of partition function in the complex temperature plane of $y = e^{\beta J}$ [3–5], i.e., Fisher zeros, with J being the coupling strength of spins. Particularly for the Ising model, Fisher zeros lie on two circles in the thermodynamic limit [6–9]. Over the years, both Lee-Yang and Fisher zeros have been extensively studied theoretically across various models [10, 11]. Experimentally, Lee-Yang zeros of the classical Ising model have been observed through detecting the quantum coherence of a probe spin coupled to an Ising-type spin bath [12, 13].

In contrast to classical phase transitions driven by thermal fluctuations, quantum phase transitions are characterized by non-analytic changes in ground states and are driven by quantum fluctuations arising from the Heisenberg uncertainty principle [14–16]. The advent of advanced experimental techniques has recently elevated the study of quantum phase transitions to a focal point in both statistical and condensed matter physics [17–21]. As such, to understand quantum phase transitions through the lens of generalized partition functions has emerged as a compelling topic. In general, a d -dimensional quantum model can be mapped into a $(d + 1)$ -dimensional classical model [14, 15, 22–24]. In light of this quantum-classical mapping, both concepts of Lee-Yang zeros and Fisher zeros, originally formulated for classical systems, can be generalized to quantum systems and to characterize

quantum phase transitions: the former refers to introduce a complex symmetry-breaking term, analogous to the Lee-Yang case [25]; whereas the latter is associated with a complex quantum fluctuation term, e.g., the complex transverse field for quantum Ising models [26–28]. The complex quantum fluctuation serves as the counterpart of the Fisher’s complex inverse temperature according to the quantum-classical mapping.

Although quantum phase transitions are inherently zero-temperature phenomena, natural systems and their measurements inevitably exist at non-zero temperatures, as dictated by the third law of thermodynamics. In this context, temperature serves as more than just an auxiliary variable alongside the Hamiltonian parameters; it acts as an additional ‘imaginary-time’ dimension that intricately weaves together static and dynamic scaling properties in a realm called the quantum critical regime (critical fan) [14, 23, 29]. In such a regime, the interplay between quantum and thermal fluctuations manifests in a range of fascinating physical effects similar to those of strongly correlated systems [14, 30].

Motivated by the fundamental roles of Lee-Yang and Fisher zeros, as well as the essentiality of the temperature in quantum criticality, in the present work, we introduce a new extension of the partition function for quantum models, termed the *imaginary-temperature partition function*, defined as

$$Z(iT, \lambda) = \text{Tr} \left[e^{-\frac{H(\lambda)}{iT}} \right], \quad (1)$$

where H is the Hamiltonian, λ is a certain parameter that can trigger a zero-temperature phase transition, and iT indicates the *imaginary temperature*. Our investigations focus on the zeros of $Z(iT, \lambda)$. At first glance, our extension seems akin to Fisher’s extension on the inverse temperature. However, this is not the case. According to the quantum-classical mapping, Eq. (1) represents the imaginary generalization of the extra dimension, thereby featuring a fundamentally different physical meaning from the Fisher’s framework. To distinguish it from the latter, we term the zeros of $Z(iT, \lambda)$ as the *imaginary-temperature zeros* (ITZs).

We take the transverse-field Ising (TFI) chain as an example, a model renowned for hosting an Ising-class quantum phase transition. Before engaging in the specifics, we list the key findings of this paper as follows. 1) In the λ - T plane, the ITZs can be categorized into distinct *zero sectors*. Within each sector, the ITZs can be arranged on a unit circle of $z = e^{i2\pi T/w}$, where w is the width of spread of zeros along the T direction. 2) The distribution of ITZs are different among various phases, demonstrating that ITZs are capable to probe the occurrence of the ground-state phase transition. 3) Near sector's boundaries, both the density of zeros and the magnetization exhibit universal singular behaviors. Notably, the longitudinal magnetization can signify the critical exponents of the Ising universality class. 4) We elucidate the relationship between the ITZs and the zeros of spectrum form fact within the context of quantum dynamics, which provides a potential experimental avenue for the realization of ITZs.

Model and Spectrum. The Hamiltonian of the TFI chain reads

$$H = - \sum_{j=1}^{N-1} \sigma_j^z \sigma_{j+1}^z - \lambda \sum_{j=1}^N \sigma_j^x, \quad (2)$$

where $\sigma_j^{\{x,z\}}$ represent the spin-1/2 Pauli operators at site j , and N is the chain length. The first term of H accounts for the nearest spin-spin interaction with unit strength, and the second term characterizes the transverse field of strength λ . The model undergoes a second-order quantum phase transition at $\lambda = 1$ [14, 29, 31]. For $\lambda < 1$, the ground states are ferromagnetic with two-fold degeneracy; for $\lambda > 1$, the ground state is paramagnetic with no degeneracy.

The spectrum of the TFI chain can be obtained in the quasi-particle space. After the Jordan-Wigner transformation and the Bogoliubove transformation, H can be diagonalized as $H_f = \sum_q \epsilon_q (2\eta_q^\dagger \eta_q - 1)$, where η_q denote the quasi-particle operators, and ϵ_q is the quasi-particle dispersion given by

$$\epsilon_q = \sqrt{1 + \lambda^2 + 2\lambda \cos q}, \quad (3)$$

which is gapless at the critical point $\lambda = 1$, and gapped otherwise. For finite N , q_j are determined by the transcendental equation $\sin[(N+1)q]/\sin(Nq) = -\lambda^{-1}$: in the paramagnetic phase with $\lambda > 1$, N real roots exist; in the ferromagnetic phase with $\lambda < 1$, there are $N-1$ real q_j and a complex π -mode with $q_N = \pi + iq'$ [31–33]. The energy of the complex mode is

$$\epsilon_{q_N} = \sqrt{1 + \lambda^2 - 2\lambda \cosh q'}. \quad (4)$$

In the thermodynamic limit, $\lim_{N \rightarrow \infty} \epsilon_{q_N} \sim \lambda^N (1 - \lambda^2) \rightarrow 0$ [34], signifying the existence of a pair of Majorana zero states in the ferromagnetic phase [35, 36].

ITZs for the TFI chain. We calculate the ITZs for the TFI chain. The imaginary-temperature partition function $Z(iT, \lambda)$ can be obtained based on Eq. (1), which takes all the many-body eigen-energies E_n into account. According to H_f , the

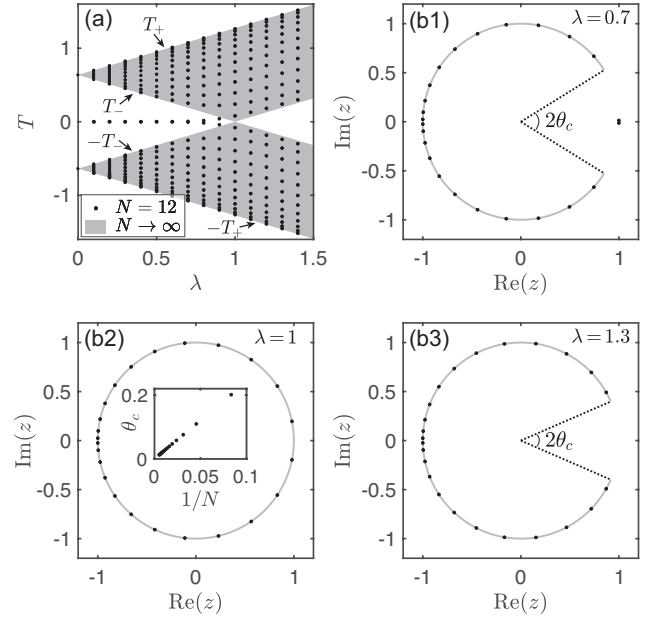


FIG. 1. (a) ITZs in the $m = 1$ zero sector. Discrete dots are obtained by numerics with $N = 12$, and the shading indicates the bounded area where ITZs exist in the thermodynamic limit $N \rightarrow \infty$. (b) ITZs distributed on the complex plane of z , where dots and shading lines correspond to the results for $N = 12$ and $N \rightarrow \infty$. Panels (b1)-(b3) show cases $\lambda = 0.7$, $\lambda = 1$, and $\lambda = 1.3$, respectively. The inset of (b2) displays the scaling behavior of θ_c on $1/N$.

energies can be expressed as $E_n = \sum_q s_q^n \epsilon_q$, with $s_q^n = \{1, -1\}$ indicating the occupation or vacuum of the q -mode. In particular, the ground state is with $s_q^0 = -1$ for all q , and $E_0 = -\sum_q \epsilon_q$, i.e., all quasi-particle modes are vacuum. Then, the partition function can be explicitly carried out as

$$Z(iT, \lambda) = \sum_{\{s_q\}} e^{-\frac{\sum_q s_q^n \epsilon_q}{iT}} = 2^N \prod_q \cos\left(\frac{\epsilon_q}{T}\right), \quad (5)$$

where $\{s_q\}$ represents the sum over all possible occupation configurations. Eq. (5) reveals that an ITZ would appear when any q -mode satisfies $\epsilon_q/T^* = \pm m\pi/2$, or equivalently,

$$T^* = \pm \frac{2\epsilon_q}{m\pi} = \pm \frac{2\sqrt{1 + \lambda^2 + 2\lambda \cos q}}{m\pi}, \quad (6)$$

where $m = \{1, 3, 5, \dots\}$ is an odd integer. Note that m divides the zeros into distinct *zero sectors*. Within each sector, there are $2N$ ITZs: N for $T > 0$, and N for $T < 0$. The distribution of ITZs are symmetric about the $T = 0$ axis.

In Fig. 1(a), we illustrate the first zero sector ($m = 1$) in the λ - T plane, where discrete dots represent numerical results for a finite system with $N = 12$. According to Eq. (6), all other zero sectors with $m \neq 1$ (shown in the Supplemental Materials [34]) would exhibit an identical structural pattern to that of the first sector, albeit rescaled by a factor of $1/m$ along the T axis. Since $\cos q \in [-1, 1]$, T^* with respect to the real- q modes are bounded within edges. Specifically for $T > 0$, the

edges are figured out as

$$T_{\pm} = \frac{2|1 \pm \lambda|}{m\pi}, \quad (7)$$

where \pm respectively denote the upper and lower edges, as shown in Fig. 1(a). For $T < 0$, the edges pick up a minus sign. In the thermodynamic limit where the real- q becomes continuous, the ITZs are continuously distributed within the range $T^* \in \pm[T_-, T_+]$, which are indicated by the shaded areas in Fig. 1(a).

In the paramagnetic phase with $\lambda > 1$, all ITZs fall into the bounded regime. At the critical point $\lambda = 1$, the lower edge of all sectors converge to the horizontal axis $T_- = 0$, serving as a hallmark of the quantum phase transition. The convergence is attributable to the gap closing of the bulk spectrum [Eq. (3)] at the critical point: a gapless ϵ_q results in an ITZ at $T^* = 0$, as per Eq. (6). In the ferromagnetic phase $\lambda < 1$, there exist two isolated lines of ITZs proximate to the horizontal axis, as shown in Fig. 1(a), which arises from the complex π -modes q_N . In the thermodynamic limit, these ITZs precisely align with the horizontal axis, owing to $\epsilon_{q_N} \rightarrow 0$. Therefore, the unique features of ITZs provide explicit diagnosis on various phases and the phase transition.

In a manner analogous to the aforementioned Lee-Yang circle $x = e^{\beta h}$ and Fisher's circle $y = e^{\beta J}$, our ITZs can also be formulated on a unit circle

$$z \equiv e^{i\frac{2\pi T}{w}}, \quad (8)$$

where $w \equiv 2T_+$ is the width of the ITZs distribution along the T axis. We display the ITZs in the complex z -plane in Fig. 1(b), where panels (b1)-(b3) correspond to the cases $\lambda = 0.7, 1$, and 1.3 , respectively. Again, discrete points are the results for $N = 12$, while the shading lines are the results for $N \rightarrow \infty$. For $\lambda \neq 1$, the circle is open, with edges $\pm\theta_c$ corresponding to the lower edges $\pm T_-$ in Fig. 1(a). Particularly for the ferromagnetic phase [Fig. 1(b1)], isolated ITZs exist within the opening. At the critical point $\lambda = 1$ [Fig. 1(b2)], the edges tends to close. The inset of Fig. 1(b2) presents the scaling of $\pm\theta_c$ on N , which clearly illustrates the closing behavior of edges in the thermodynamic limit.

Edge Singularities. One of the captivating aspects of Lee-Yang theory is the Yang-Lee edge singularity, which refers to the universal scaling of the Lee-Yang zeros' density ρ near the boundary h_c , i.e., $\rho \propto (h - h_c)^\sigma$ with σ the exponent. Fisher pointed out that the Yang-Lee edge singularity is actually a critical phenomenon described by a field theory with imaginary cubic interaction [9]. Up to now, the Yang-Lee edge singularity has shed light on such fields as high-energy physics [37, 38], non-Hermitian systems [39], universal properties in first-order phase transition [40, 41], etc. This prompts us to explore the singular phenomena of the ITZs.

We identify two distinct types of singular behaviors: the first type is associated with the density of ITZs, characterized by an exponent $\sigma_1 = -1/2$, in contrast to the well-known Yang-Lee edge singularity $\sigma = -1/6$ for TFI model [42];

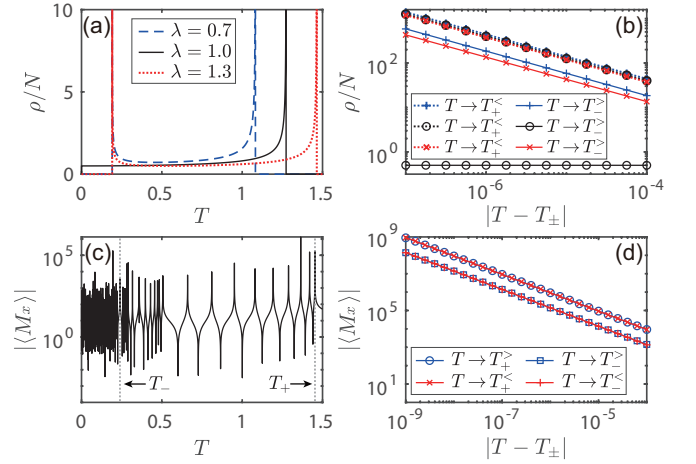


FIG. 2. (a) ITZs' density distribution $\rho(T)$ of the $m = 1$ sector within $T \geq 0$. (b) Scaling behavior of $\rho(T)$ near the sector edges $T = T_{\pm}$, where $T^<$ and $T^>$ denote approaches to the edges from the left and right, respectively. (c) Transverse magnetization M_x as a function of T , with dotted lines indicating the edge locations of the $m = 1$ sector. (d) Scaling of the singularities in M_x near the edges.

the second type pertains to the divergence of the transverse magnetization with exponent $\sigma_2 = -1$. In the following, we will discuss these singularities in detail.

In the thermodynamic limit, the density of ITZs in a single sector can be analytically derived as [34]

$$\rho(T) = \frac{2NT}{\pi} |(T^2 - T_+^2)(T^2 - T_-^2)|^{-1/2} \quad (9)$$

for T within the bounded regions $\pm[T_-, T_+]$, and $\rho(T) = 0$ elsewhere. It indicates that the density of ITZs diverges at sector edges $\rho(T) \propto |T - T_{\pm}|^{\sigma_1}$ with exponent $\sigma_1 = -1/2$. Notably, both the edge singularities and the exponent σ_1 are independent of λ , except at the critical point $\lambda = 1$. At the critical point, $\rho(T)$ only diverges at the upper boundary T_+ (with the same exponent $\sigma_1 = -1/2$), while maintaining a finite density $\rho(0) = N/2$ at the lower boundary $T_- = 0$. The latter is confirmed by

$$\lim_{T \rightarrow 0} \rho(T) = \lim_{T \rightarrow 0} \frac{2N}{\pi |T^2 - T_+^2|^{1/2}} = \frac{N}{2}. \quad (10)$$

In Fig. 2(a), we plot $\rho(T)$ for the cases $\lambda = 0.7, 1$, and 1.3 by various line styles. Furthermore, Fig. 2(b) specifically shows the scaling behaviors of $\rho(T)$ near the edges $T = T_{\pm}$ for the corresponding λ of Fig. 2(a). In these figures, one can clearly observe the distinction between critical and non-critical cases, as well as the singular exponent $\sigma_1 = -1/2$.

Now, we turn to the magnetization defined as [according to Eq. (1)]

$$M_{x,z}(T) = \frac{\text{Tr} \left[e^{-\frac{H}{iT}} S_{x,z} \right]}{Z(iT, \lambda)} = \frac{\sum_n e^{-\frac{E_n}{iT}} \langle n | S_{x,z} | n \rangle}{Z(iT, \lambda)}, \quad (11)$$

where $S_{x,z} = N^{-1} \sum_j \sigma_j^{x,z}$. In contrast to the Lee-Yang theory which is symmetry breaking [9], our longitudinal magnetization M_z is always vanishing since the partition function $Z(iT, \lambda)$ respects the spin-flip symmetry. For the transverse magnetization M_x , the numerator of Eq. (11) is smooth and differentiable for $T > 0$; likewise, the denominator $Z(iT, \lambda)$ is also a smooth function, albeit with zeros. This suggests that the singular points in $M_x(T)$ should coincide with the ITZs, as shown in Fig. 2(b1). Furthermore, by expanding $Z(iT, \lambda)$ near T_{\pm} , we find that $M_x(T)$ diverges as $M_x(T) \propto |T - T_{\pm}|^{\sigma_2}$ with $\sigma_2 = -1$ [34], as illustrated in Fig. 2(b2). The exponent σ_2 is the second scaling exponent observed in our system.

Relation to the Spectrum Form Factor. The imaginary-temperature partition function carries an additional layer of physical meaning in the context of quantum dynamics. To elucidate this, we consider the modula

$$|Z(iT, \lambda)|^2 = \left| \sum_n \langle n | e^{i\frac{\hbar}{T}} | n \rangle \right|^2 = D^2 |\langle \Psi_0 | e^{-i\frac{\hbar}{T}} | \Psi_0 \rangle|^2, \quad (12)$$

where $|\Psi_0\rangle = D^{-1/2} \sum_n |n\rangle$, and $D = 2^N$ denotes the dimension of Hilbert space. Clearly, by setting $t \sim 1/T$, $|Z(t)|^2$ represents the return probability when the initial state $|\Psi_0\rangle$ is an equally weighted superposition of all eigenstates. The return probability essentially links to the spectral form factor (SFF) [43–50] in the manner of

$$K(t) = \frac{1}{D} \left\langle \left| \sum_E g(E) e^{-i2\pi Et} \right|^2 \right\rangle = \frac{|Z(2\pi t)|^2}{D}, \quad (13)$$

with $g(E)$ the density of state, and $\langle \dots \rangle$ denotes the average on a spectral ensemble. For the current system, the entire spectrum can be precisely solved, rendering the ensemble average irrelevant. Therefore, up to the factor D , there is an one-to-one correspondence between the ITZs and the zeros of the SFF, satisfying $t^* = 1/2\pi T^*$.

Commonly, the envelope structure of SFF can be used to distinguish various quantum states. For example, in chaotic systems, the SFF displays a three-stage 'slope-ramp-plateau' structure [43–50], with the two characteristic time scales as the Thouless time and Heisenberg time; the ratio of the two time scales can further be used to assess the ergodicity breaking. Here, we emphasize that the zeros of $K(t)$ offer important information in signifying quantum phase transitions.

In Fig. 3(a), we present the numerical result of $K(t)$ for $N = 12$ and $\lambda = 1$. The plot also reveals a three-stage behavior. Prior to the timescale $t_s = 1/4(1 + \lambda)$, $K(t)$ declines smoothly devoid of zeros. This stage corresponds to T decreasing from infinity down to the upper boundary T_+ of the $m = 1$ sector. After t_s , $K(t)$ manifests a plethora of zeros. We have verified that the indicated zeros of $K(t)$ [by the vertical dotted lines in Fig. 3(a)] strictly correspond to the ITZs of the $m = 1$ sector [see Fig. 1(a)], satisfying $t^* = 1/2\pi T^*$. Other unindicated zeros of $K(t)$ correspond to the ITZs in other sectors. For sufficiently large t , $K(t)$ stabilizes at a plateau ~ 1 ,

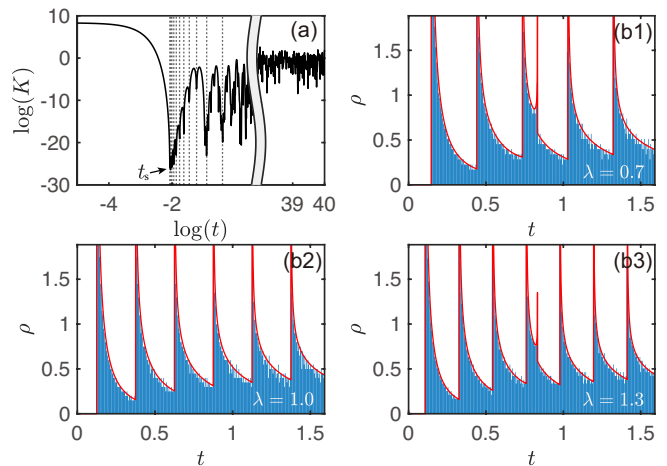


FIG. 3. (a) Log-log plot of the SFF $K(t)$ for $N = 12$ and $\lambda = 1$. Vertical dotted lines verify the one-to-one correspondence between the zeros of $K(t)$ and the ITZs in the $m = 1$ sector shown in Fig. 1(a). (b) Density distribution of the zeros of $K(t)$. Solid lines denote analytical results in the thermodynamic limit, while bars are derived from numerical statistics for $N = 10^3$. Panels (b1)-(b3) correspond to the cases of $\lambda = 0.7$, $\lambda = 1$, and $\lambda = 1.3$, respectively.

as anticipated, signifying the time scale beyond the Heisenberg time.

Examining the zero density $\rho(t)$ of the SFF helps to identify the critical point. As mentioned before, at the critical point $\lambda = 1$, the density of ITZs only diverges at the upper boundary T_+ of all zero sectors. Consequently, the zero density $\rho(t)$ manifests periodic peaks, as shown in Fig. 3(b2), in a period of $2t_s$. In contrast, for the non-critical cases $\lambda \neq 1$, additional peaks emerge, as illustrated in Fig. 3(b1) and (b3). These additional peaks originate from the singularities at the lower boundaries T_- . In Fig. 3(b), solid lines delineates the analytical results in the thermodynamic limit based on Eq. (9), whereas the bars represent the numerical statistical results for $N = 10^3$. The analytical and numerical results are in excellent agreement.

Discussion. We finally turn to another crucial question: Can ITZs signify the intrinsic critical exponents of the Ising universality class? The short answer is Yes. In fact, a detailed exposition of this question will be the central focus of our forthcoming work. Here, we provide a glimpse.

At first, the bounded region of ITZs for $T > 0$, shown in Fig. 1(a), can be treated as a 'critical fan'. In this sense, near $\lambda = 1$, the lower edge T_- should be governed by the conventional zero-temperature partition function. According to critical theory [14], T_- should satisfy $T_- \propto (\lambda - 1)^{\nu s}$, where ν and s are the correlation length exponent and the dynamic exponent, respectively. For the Ising universality class, $\nu = 1$ and $s = 1$, yielding $T_- \propto (\lambda - 1)$, which confirms Eq. (7).

Furthermore, probing the system by a weak longitudinal magnetic field $-h \sum_j \sigma_j^z$ leads to a non-vanishing $M_z(T)$ [defined in Eq. (11)], which is shown in Fig. 4(a). We find that, near $\lambda = 1$, the behavior of M_z at the lower edge $T = T_-$ is

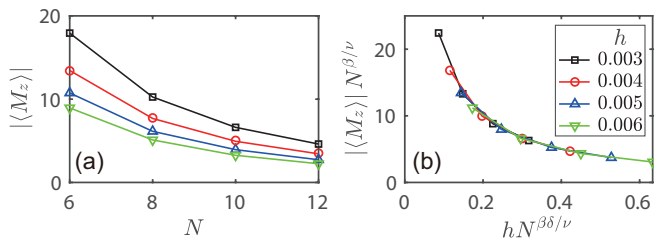


FIG. 4. (a) Longitudinal magnetization M_z as a function of N , with $(\lambda - 1)L = 0.1$ being fixed. (b) Rescaled plot of M_z and N , where all curves collapse onto each other. In both panels, various markers denote cases corresponding to different probe field strengths h .

determined by the Ising critical exponents, i.e.,

$$M_z(T_-) = N^{-\beta/\nu} f[(\lambda - 1)N^{1/\nu}, hN^{\beta\delta/\nu}, T_-(\lambda - 1)^{-\nu s}], \quad (14)$$

where f is the scaling function, and $\beta = 1/8$, $\delta = 15$ are the Ising exponents of the magnetization and the response exponent to external field, respectively. Therefore, for a fixed $(\lambda - 1)N^{1/\nu}$, by rescaling M_z and N into $M_z N^{\beta/\nu}$ and $hN^{\beta\delta/\nu}$, all the curves should match with each other, which is numerically confirmed in Fig. 4(b).

Conclusion. In this paper, we have investigated a new type of zeros, termed by ITZs, in the quantum Ising model. These zeros are defined as the roots of the imaginary-temperature partition function. Our results not only revealed an intimate relation between the ITZs and quantum criticality, but also elucidated the correspondence between ITZs and the zero points of spectral form factor. The latter can serve as a dynamical scheme for detecting both ITZs and quantum criticality. Our findings are expected to provide a novel insight into the statistical characterization of zero-temperature phase transitions, and may also have implications for the relevant experiments.

J. L. and L. C. would like to thank Markus Heyl for insightful discussion. L. C. acknowledges supports from the NSF of China (Grants No. 12174236) and from the fund for the Shanxi 1331 Project. S. Y. is supported by the NSF of China (Grants No. 12222515 and No. 12075324).

* yinsh6@mail.sysu.edu.cn

† lchen@sxu.edu.cn

- [1] C. N. Yang and T. D. Lee, Statistical Theory of Equations of State and Phase Transitions. I. Theory of Condensation, Phys. Rev. **87**, 404 (1952).
- [2] T. D. Lee and C. N. Yang, Statistical Theory of Equations of State and Phase Transitions. II. Lattice Gas and Ising Model, Phys. Rev. **87**, 410 (1952).
- [3] M. E. Fisher, The Nature of Critical Points, Lectures Notes in Theoretical Physics edited by W. E. Brittin (University of Colorado Press, 1965), 7c.
- [4] W. T. Lu and F. Y. Wu, Density of the Fisher Zeroes for the Ising Model, J. Stat. Phys. **102**, 953 (2001).

- [5] M. Heyl, Dynamical Quantum Phase Transitions: A Review, Rep. Prog. Phys. **81**, 054001 (2018).
- [6] S.-Y. Kim, Fisher Zeros of the Ising Antiferromagnet in an Arbitrary Nonzero Magnetic Field, Phys. Rev. E **71**, 017102 (2005).
- [7] S. Katsura, Distribution of Roots of the Partition Function in the Complex Temperature Plane, Prog. Theor. Phys. **38**, 1415 (1967).
- [8] H. J. Brascamp and H. Kunz, Zeroes of the Partition Function for the Ising Model in the Complex Temperature Plane, J. Math. Phys. **15**, 65 (1974).
- [9] M. E. Fisher, Yang-Lee Edge Singularity and ϕ^3 Field Theory, Phys. Rev. Lett. **40**, 1610 (1978).
- [10] B.-B. Wei and R.-B. Liu, Lee-Yang Zeros and Critical Times in Decoherence of a Probe Spin Coupled to a Bath, Phys. Rev. Lett. **109**, 185701 (2012).
- [11] J. Liu, A. Sinclair, and P. Srivastava, Fisher Zeros and Correlation Decay in the Ising Model, J. Math. Phys. **60**, 103304 (2019).
- [12] X. Peng, H. Zhou, B.-B. Wei, J. Cui, J. Du, and R.-B. Liu, Experimental Observation of Lee-Yang Zeros, Phys. Rev. Lett. **114**, 010601 (2015).
- [13] C. Binek, W. Kleemann, and H. A. Katori, Yang-Lee Edge Singularities Determined from Experimental High-Field Magnetization Data, J. Phys.: Condens. Matter **13**, L811 (2001).
- [14] S. Sachdev, Quantum Phase Transitions (Cambridge University Press, Cambridge, England, 1999).
- [15] S. L. Sondhi, S. M. Girvin, J. P. Carini, and D. Shahar, Continuous Quantum Phase Transitions, Rev. Mod. Phys. **69**, 315 (1997).
- [16] M. Vojta, Quantum Phase Transitions, Rep. Prog. Phys. **66**, 2069 (2003).
- [17] G. Jotzu, M. Messer, R. Desbuquois, M. Lebrat, T. Uehlinger, D. Greif, and T. Esslinger, Experimental Realization of the Topological Haldane Model with Ultracold Fermions, Nature **515**, 237 (2014).
- [18] N. Fläschner, B. S. Rem, M. Tarnowski, D. Vogel, D.-S. Lühmann, K. Sengstock, and C. Weitenberg, Experimental Reconstruction of the Berry Curvature in a Floquet Bloch Band, Science **352**, 1091 (2016).
- [19] I. Bloch, J. Dalibard, and W. Zwerger, Many-Body Physics with Ultracold Gases, Rev. Mod. Phys. **80**, 885 (2008).
- [20] M. Lewenstein, A. Sanpera, V. Ahufinger, B. Damski, A. Sen(De), and U. Sen, Ultracold Atomic Gases in Optical Lattices: Mimicking Condensed Matter Physics and Beyond, Adv. Phys. **56**, 243 (2007).
- [21] M. Greiner, O. Mandel, T. Esslinger, T. W. Hänsch, and I. Bloch, Quantum Phase Transition from a Superfluid to a Mott Insulator in a Gas of Ultracold Atoms, Nature **415**, 39 (2002).
- [22] P. Pfeuty, The Quantum-Classical Crossover Critical Behaviour of the Ising Model in a Transverse Field, J. Phys. C: Solid State Phys. **9**, 3993 (1976).
- [23] S. Chakravarty, B. I. Halperin, and D. R. Nelson, Low-Temperature Behavior of Two-Dimensional Quantum Antiferromagnets, Phys. Rev. Lett. **60**, 1057 (1988).
- [24] A. M. Polyakov, Gauge Fields and Strings (Harwood Academic Publishers, Chur, Switzerland; New York, 1987).
- [25] S. Yin, G.-Y. Huang, C.-Y. Lo, and P. Chen, Kibble-Zurek Scaling in the Yang-Lee Edge Singularity, Phys. Rev. Lett. **118**, 065701 (2017).
- [26] R. A. Blythe and M. R. Evans, The Lee-Yang Theory of Equilibrium and Nonequilibrium Phase Transitions, Braz. J. Phys. **33**, 464 (2003).
- [27] I. Bena, M. Droz, and A. Lipowski, Statistical mechanics

- of equilibrium and nonequilibrium phase transitions: The Yang–Lee formalism, *Int. J. Mod. Phys. B* **19**, 4269 (2005).
- [28] B.-B. Wei, S.-W. Chen, H.-C. Po, and R.-B. Liu, Phase Transitions in the Complex Plane of Physical Parameters, *Sci Rep* **4**, 5202 (2014).
- [29] A. Dutta, *Quantum Phase Transitions in Transverse Field Spin Models: From Statistical Physics to Quantum Information* (Cambridge University Press, Delhi, India, 2015).
- [30] A. Mann, M. Revzen, H. Umezawa, and Y. Yamanaka, Relation between Quantum and Thermal Fluctuations, *Phys. Lett. A* **140**, 475 (1989).
- [31] P. Pfeuty, The One-Dimensional Ising Model with a Transverse Field, *Ann. Phys.* **57**, 79 (1970).
- [32] G. G. Cabrera and R. Jullien, Role of Boundary Conditions in the Finite-Size Ising Model, *Phys. Rev. B* **35**, 7062 (1987).
- [33] Y. He and H. Guo, The Boundary Effects of Transverse Field Ising Model, *J. Stat. Mech.* **2017**, 093101 (2017).
- [34] See the Supplemental Materials for more detailed information.
- [35] K. Chhajed, From Ising Model to Kitaev Chain – An Introduction to Topological Phase Transitions, *Reson* **26**, 1539 (2021).
- [36] N. Seiberg and S.-H. Shao, Majorana Chain and Ising Model – (Non-Invertible) Translations, Anomalies, and Emanant Symmetries, arXiv: 2307.02534 (2023).
- [37] W. Li, Taming Dyson-Schwinger Equations with Null States, *Phys. Rev. Lett.* **131**, 031603 (2023).
- [38] P. Dimopoulos, L. Dini, F. Di Renzo, J. Goswami, G. Nicotra, C. Schmidt, S. Singh, K. Zambello, and F. Ziesché, Contribution to Understanding the Phase Structure of Strong Interaction Matter: Lee-Yang Edge Singularities from Lattice QCD, *Phys. Rev. D* **105**, 034513 (2022).
- [39] C. M. Bender, Making Sense of Non-Hermitian Hamiltonians, *Rep. Prog. Phys.* **70**, 947 (2007).
- [40] F. Zhong and Q. Chen, Theory of the Dynamics of First-Order Phase Transitions: Unstable Fixed Points, Exponents, and Dynamical Scaling, *Phys. Rev. Lett.* **95**, 175701 (2005).
- [41] F. Zhong, Imaginary Fixed Points Can Be Physical, *Phys. Rev. E* **86**, 022104 (2012).
- [42] J. L. Cardy, Conformal Invariance and the Yang-Lee Edge Singularity in Two Dimensions, *Phys. Rev. Lett.* **54**, 1354 (1985).
- [43] C. B. Dağ, S. I. Mistakidis, A. Chan, and H. R. Sadeghpour, Many-Body Quantum Chaos in Stroboscopically-Driven Cold Atoms, *Commun Phys* **6**, 1 (2023).
- [44] J. Šuntajs, J. Bonča, T. Prosen, and L. Vidmar, Quantum Chaos Challenges Many-Body Localization, *Phys. Rev. E* **102**, 062144 (2020).
- [45] G. Bunin, L. Foini, and J. Kurchan, Fisher Zeroes and the Fluctuations of the Spectral Form Factor of Chaotic Systems, arXiv:2207.02473 (2022).
- [46] A. Prakash, J. H. Pixley, and M. Kulkarni, Universal Spectral Form Factor for Many-Body Localization, *Phys. Rev. Res.* **3**, L012019 (2021).
- [47] X. Chen and A. W. W. Ludwig, Universal Spectral Correlations in the Chaotic Wave Function and the Development of Quantum Chaos, *Phys. Rev. B* **98**, 064309 (2018).
- [48] M. Winer and B. Swingle, The Loschmidt Spectral Form Factor, *J. High Energ. Phys.* **2022**, 137 (2022).
- [49] P. Kos, M. Ljubotina, and T. Prosen, Many-Body Quantum Chaos: Analytic Connection to Random Matrix Theory, *Phys. Rev. X* **8**, 021062 (2018).
- [50] M. Schiulaz, E. J. Torres-Herrera, and L. F. Santos, Thouless and Relaxation Time Scales in Many-Body Quantum Systems, *Phys. Rev. B* **99**, 174313 (2019).